



This is a repository copy of *Cost-competitive manufacture of porous-silicon anodes via the magnesiothermic reduction: a techno-economic analysis*.

White Rose Research Online URL for this paper:

<https://eprints.whiterose.ac.uk/204075/>

Version: Accepted Version

Article:

Yan, M., Martell, S., Dasog, M. et al. (2 more authors) (2023) Cost-competitive manufacture of porous-silicon anodes via the magnesiothermic reduction: a techno-economic analysis. *Journal of Power Sources*, 588. 233720. ISSN 0378-7753

<https://doi.org/10.1016/j.jpowsour.2023.233720>

© 2023 The Authors. Except as otherwise noted, this author-accepted version of a journal article published in *Journal of Power Sources* is made available via the University of Sheffield Research Publications and Copyright Policy under the terms of the Creative Commons Attribution 4.0 International License (CC-BY 4.0), which permits unrestricted use, distribution and reproduction in any medium, provided the original work is properly cited. To view a copy of this licence, visit <http://creativecommons.org/licenses/by/4.0/>

Reuse

This article is distributed under the terms of the Creative Commons Attribution (CC BY) licence. This licence allows you to distribute, remix, tweak, and build upon the work, even commercially, as long as you credit the authors for the original work. More information and the full terms of the licence here:

<https://creativecommons.org/licenses/>

Takedown

If you consider content in White Rose Research Online to be in breach of UK law, please notify us by emailing eprints@whiterose.ac.uk including the URL of the record and the reason for the withdrawal request.



eprints@whiterose.ac.uk
<https://eprints.whiterose.ac.uk/>

Cost-competitive manufacture of porous-silicon anodes via the magnesiothermic reduction: a techno-economic analysis

Maximilian Yan^{a,b}, Sarah Martell^b, Mita Dasog^b, Solomon Brown^a and Siddharth V. Patwardhan^{a*}

^a *Department of Chemical and Biological Engineering, The University of Sheffield, Mappin Street, Sheffield S1 3JD, United Kingdom.*

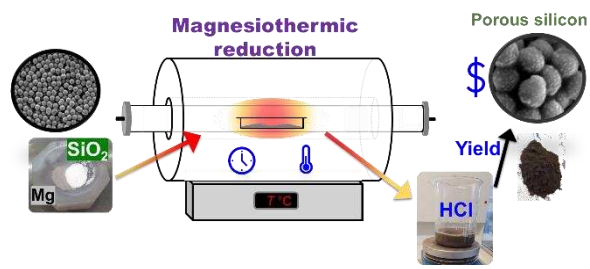
^b *Department of Chemistry, Dalhousie University, 6274 Coburg Road, Halifax, NS B3H 4R2, Canada.*

** Corresponding author, s.patwardhan@sheffield.ac.uk*

Abstract

Lithium-ion batteries play a central role in the electrification of our energy systems however this technology still suffers from low energy density. Porous silicon (p-Si) has been recognised as a promising, high-energy density anode material as a replacement for the currently used graphite. The demand for p-Si is therefore expected to increase in the coming decades and the magnesiothermic reduction (MgTR) has shown great promise as a scalable process that can be used to meet this demand. However, without a preliminary or detailed economic analysis, it is not possible to determine whether this process is economically feasible at larger scales, under conditions that have thus been reported in the literature. Herein, as a first of a kind study, the total cost of production (TCOP) at scales between 300-1500kg/batch are calculated using experimentally verified data. Fixed costs make up the greatest proportion of TCOP, at 58% of the TCOP at the largest scale, with a payback time of 10 years. Total variable costs (feedstock and energy) was 42% of the TCOP. When recently reported modifications to MgTR – a two-step and ultra-low temperature methods – were considered, the variable costs reduced by ~40% and ~32% respectively, and reducing the TCOP for the two-step and low-temperature methods by 45% and 37% respectively. When the cost of producing p-Si through the MgTR process was compared to that of graphite on a “capacity cost” basis (\$/Ah), it was clear that p-Si produced via MgTR process rivals the market price of graphite. These results provide the first evidence that the MgTR is a highly competitive and scalable process for producing anode grade porous silicon. The variable costs can be lowered in the future by changing the conditions, and the most effective ways to do this are presented in this study.

Graphical table of contents



[parameters in blue were optimised]

1. Introduction

In the shift towards a net zero carbon economy, the demand for high energy density lithium-ion batteries (LIBs) is increasing rapidly¹. Although they are currently dominating the electric vehicle market, the issue with low mileage has yet to be tackled. A typical mass market EV has a mileage of 67 kWh, equivalent to 224 Wh/kg at cell level, capable of achieving a mileage of only 168 miles in a single charge². This energy density is still far below the target of ≥ 350 Wh/kg by the year 2030 set by the US Department of Energy and the Batteries Europe strategy^{3,4}. At present, the anode material of choice is graphite, however, in order to meet these targets, higher energy density materials need to be considered. Furthermore, between 50-70% of the raw graphite is lost when it is upgraded to spherical, battery grade graphite, making it a highly inefficient process, thus multiplying demand and raising supply chain issues⁵.

Silicon is the most promising anode material because it possesses a high specific capacity of 3579 mAh/g⁶ and is produced from silica, an abundant feedstock. This high capacity is accompanied by a large volume expansion during charge, which has negative implications on its cyclability and safety⁷. Despite these challenges, various strategies have been proven to be effective at incorporating silicon into LIBs. These include adding silicon to graphite⁸, using elastic self-healing binders⁹, and limiting the expansion by choosing a narrowed operating voltage window¹⁰. With regards to the structure of the silicon material itself, porous structures have been shown to outperform their non-porous counterparts, as the void space allows for the material to expand without the associated mechanical stress¹¹. To achieve this, structures such as nanowires¹² and nanotubes¹³ and many more have been synthesised and these materials were able to retain a high capacity after the initial SEI formation cycles.

Existing methods of producing nanostructured silicon present challenges when scaling up as they involve inherently slow and energy intensive processes that require specific, synthetic silicon feedstock. Pure silicon is first made by the carbothermal reduction of silica at 2000°C¹⁴. This can then be converted into wafers which are then used in etching-type (top-down) processes, or into silane gas for deposition-type (bottom-up) processes. Both methods are surface-type methods, so are energy

and resource intensive, laborious and time consuming and inherently difficult or uneconomical to scale¹⁵. A simpler, bulk process that has been heavily studied and shows great promise for scaling up p-Si production is the magnesiothermic reduction (MgTR) process. This process is able to convert a wide range of silica feedstock, raw and synthetic, directly into porous silicon (p-Si) at 650°C¹⁶.

2. Process overview

The process consists primarily of solids handling equipment with liquid handling equipment during the downstream processing steps. Dry powders of Mg and SiO₂ are mixed before being transferred into a tubular furnace and heated at a chosen temperature between 650°C and 800°C. The reaction has been shown to produce Si after 30 minutes¹⁷ but is usually held for much longer times (6 hours) to ensure reaction completion¹⁸, under an inert atmosphere. The solid mixture is then cooled and etched in aqueous HCl to remove Mg containing species, leaving behind a porous structure of Si and unreacted SiO₂. Compounds containing Mg react with HCl to form MgCl₂ which remains in solution, while solid Si and unreacted SiO₂ remain as solids suspended in the solution. After all Mg containing species have been reacted, the suspension is passed through a filter to separate the solids. A filter cake is obtained which, when dried, leaves a powder consisting of Si and unreacted SiO₂. A block flow diagram of the process is shown in Figure 1.

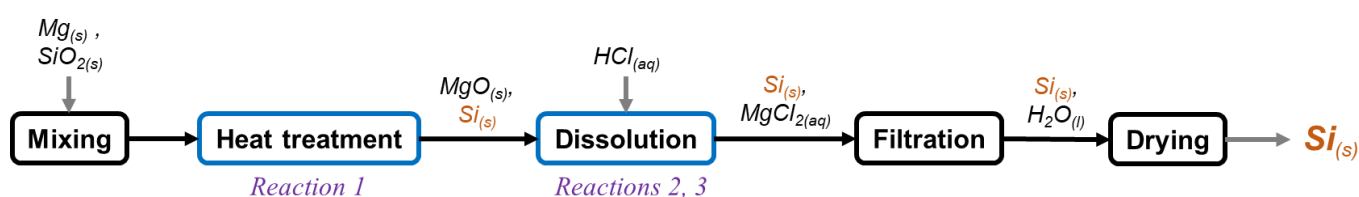
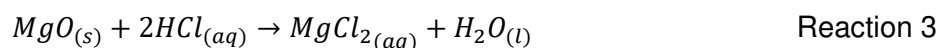
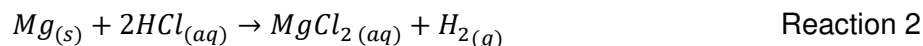
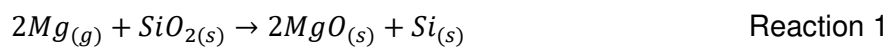


Figure 1: A block flow diagram showing the individual steps in the process. Steps which include reactions are coloured in blue. Materials/reagents input and output is shown for each step.

Under an inert atmosphere, Mg and SiO₂ undergo a redox reaction, whereby SiO₂ is reduced to Si (Reaction 1). The overall yield is defined as the moles of elemental Si divided by the total moles of Si

+ SiO₂ in the product. Any unreacted Mg and MgO produced are removed during the dissolution steps via Reaction 2 and 3 respectively.



A high yield is important as with any manufacturing process, however, the silicon produced here needs to have porosity for LIBs. Typically, the MgTR reaction carried out at 650°C for 6 hours achieves a yield of 60-70% with porosity that is desired for the electrochemical performance. Increasing the reaction temperature to 850°C achieves a yield of 90% but at a loss of porosity, while operating at 500°C to retain the porosity, decreases the yield to less than 10%¹⁹. The tension between high temperature requirement to achieve higher yields and producing silicon with desired porosity for its performance makes it difficult to improve the efficiency without sacrificing the electrochemical performance. Additionally, to improve the purity of the product, excess unreacted SiO₂ have to be removed using highly toxic HF. This is not only wasteful due to the loss of the unreacted feedstock, but also is unsafe.

Multiple ways have emerged in the literature showing that it is possible to modify the process to improve the energy efficiency of the process and the yield of p-Si produced. One such modification is the two-step process, which needs 650°C for only 30 minutes to trigger the reduction, before cooling to 300°C to carry out the reaction for 6 hours²⁰. This method is potentially advantageous economically as most of the reduction time is spent at a lower temperature, hence it is likely that less energy is required overall to maintain the temperature during the dwelling stages. Another modification to the MgTR process is to reduce the operating temperature. It was shown recently that the reaction can be carried out at 380°C by using nano-sized feedstock²¹. The likely economic benefit of this method is that the temperature of the furnace never exceeds 380°C, therefore it has the potential to minimise the overall energy consumption and cost. As a third strategy, without lowering the maximum temperature requirement, it was demonstrated that the yield at 750°C could be increased from 55% to 92% by using a rotating furnace during the reduction step to minimise mass transfer limitations²².

Other works have shown that the MgTR can produce silicon with properties that are suitable for high-capacity lithium-ion cells using low-cost feedstock such as sand²³, crushed glass²⁴, and clays²⁵.

The studies described above can help reduce or remove the tension between temperature requirement to achieve high yield and porosity needed for the electrochemical performance, thereby presenting multiple strategies for improving the process to make the MgTR more economical and increasing its viability for scale up. Despite the huge potential of MgTR for scale-up and recent process improvements, the process economics of producing silicon via the traditional MgTR method is not known. Therefore, neither the commercial viability of MgTR can be explored, nor the savings from implementing improved methods be quantified.

In this work we used factorial methods to estimate the total cost of producing p-Si via the MgTR process¹⁹. Incorporating reaction parameters for experimentally verified methods, we compared process economics for various MgTR method. The variable costs, (VC), fixed costs (FC) and total cost of production (TCOP) were estimated and analysed to gain process insights. From this information we propose potential strategies for improving the process, and the impact these improvements will have on the VC, FC and TCOP.

3. Methods

3.1 Demand and costing

To perform an economic analysis of the process including capital and operating costs, a production capacity had to be defined. The demand for porous silicon was found from strategies outlined by government organisations. In the UK, the Advanced Propulsion Centre have forecasted that the battery demand for passenger vehicles will reach 82 GWh by 2030 ²⁶. A typical mass market EV such as the Nissan Leaf is capable of storing 67 kWh in a single charge and this is equivalent to approximately 1.2 million EVs/y.

In such a vehicle, between 40-70 kg of graphite is needed for the anode ^{27,28}. The Batteries Europe Strategy has set a target of 20% of graphite anodes to be replaced by Si by 2030⁴. As a conservative estimate, the yearly silicon demand for anodes in the UK by 2030 was calculated as follows:

$$Si_{demand} = 0.1 \times \frac{kg \text{ graphite}}{EV} \times \frac{no. of EV}{year} \quad \text{Eqn. 1}$$

The amount of graphite per EV was assumed to be 70 kg, and a factor of 0.1 was applied as a conservative estimate of 10% replacement of graphite. The total demand for silicon was estimated to be 8.4 kilotonnes/year of Si. Therefore, for 1% of the market demand with 5 days/week, 50 weeks/year operation, production capacity will be 336 kg/d. A 20% replacement of graphite would equate to 672 kg/d demand of Si. This is a ballpark value used as a starting point for process cost calculations. The silicon demand is therefore dependent on the make and model of EV, the country/region considered and their governing policies. Since there is a wide range of available information on the capacity of electric vehicles at present, and the capacity will inevitably increase in the next decade, we have carried out calculations for a range of demand to account for an increase in EV battery capacity and for variations between makes and models of EVs. Predicting a demand of Si anodes in 2030 means taking into account a wide range of factors, including socio- and psychological factors such as range anxiety, ownership vs rental vs taking public transport. A predicted distribution of EV makes and models in the market would also matter – all these factors are not within the scope of this paper. Instead, to ensure that this study is not specific only to the demand scenario chosen in this paper, a range between 100 and 1500 kg/d will be considered in this economic analysis. Scheduling and equipment configuration is outside the scope of this study, so it was assumed that this quantity was produced in a single batch, and that this batch can be completed within a day. Given that each scenario had a different total completion time due to their parameters, the throughput also differed, and this difference was captured by normalising the daily production rate.

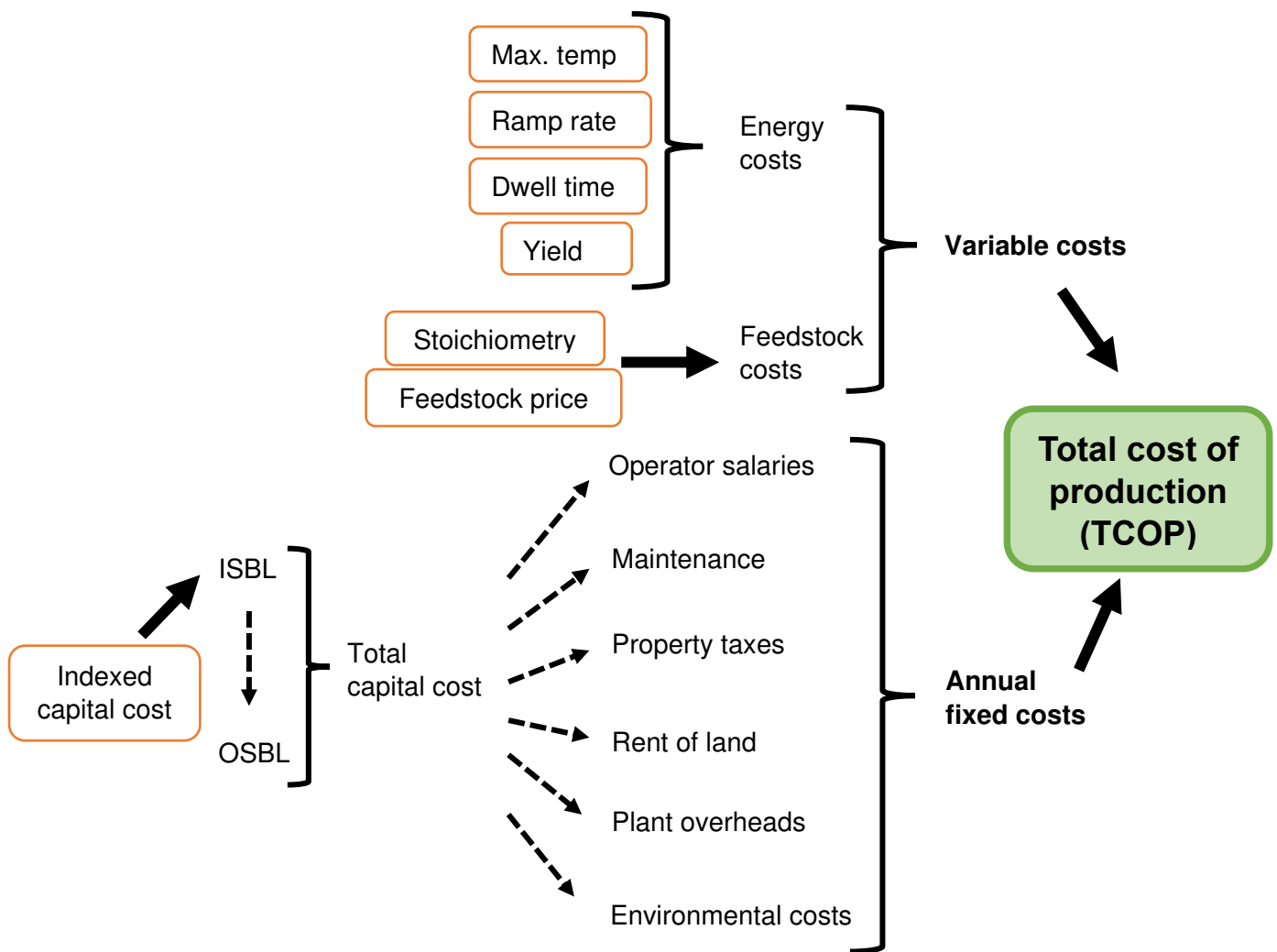


Figure 2: Procedure for calculating annual fixed costs, variable costs and the total cost of production. Orange boxes indicate variables which will be investigated in this study. Entities at the end of a dashed arrow were estimated as a percentage of the entity at the beginning of the arrow. Entities at the beginning of a solid arrow are combined to give entities at the end of the arrow.

The variable cost and annual fixed cost combined to give the total cost of production (TCOP), which was quoted in this work as \$/kg Si produced. Variable costs include energy and feedstock costs, while the annual fixed cost comes from the indexed capital cost of all the equipment. From the indexed capital cost, the total capital cost was estimated. Figure 2 summarises the procedure for calculating annual fixed cost, variable costs and TCOP. Equipment was selected according to certain criteria, which is described in the next section.

3.2 Equipment selection and indexed capital cost

Existing industrial equipment were chosen as outlined in chemical engineering equipment design literature^{29,30}, based on the physical requirements of the MgTR process (Table 1). Equipment selection was made based on key design requirements of each step of the process. The cost of each equipment was dependent on conditions of the reaction such as mole ratio of reactants, maximum temperature, dwell time, HCl concentration and yield. These corresponded to costing factors. With this information, the capital cost of the equipment was estimated from well-established factorial methods³¹. Table 1 summarises the key design requirements and costing factors for each equipment. Where available, specific costing charts and correlations were used³², otherwise, a more general costing equation was used³¹. Given the limited information available, design with this level of detail gives a “preliminary cost” and is associated an error of $\pm 30\%$ ²⁹. In all cases where only a range was available, but not exact values and percentages, estimates were made conservatively to give an overestimate of costs. The total of all equipment costs was then used to calculate the indexed capital cost. The selection and sizing of each major equipment is outlined below.

Table 1: Summary of the design requirements and factors used to estimate the cost of the equipment. The methods of energy consumption of each major equipment are also shown.

Equipment	Key design requirements	Costing factors	Method of energy consumption
Spiral ribbon powder mixer	Non-shearing, low impact	Maximum power output	Specific power requirement
Rotary kiln furnace	Reactant tumbling motion, inert atmosphere	Maximum power output	Sensible heat, heat loss (conductive, convective, radiative)
Stainless steel vessel	Corrosion resistant, agitated	Maximum volume	Specific power requirement (impeller), cooling duty
Plate filter	Suspended particles settling time, cake thickness*	Surface area	None, gravity flow filtration
Tray dryer	Low technology	Surface area	Sensible heat, latent heat

*Design requirement for the plate filter was determined from lab-scale filtration measurements.

3.3 Spiral ribbon powder mixer

From our experimental observations, mixtures of Mg and SiO₂ powders are free flowing and do not segregate. A requirement is that shear force or high impact is not applied during the mixing stage to avoid oxidation of Mg, or premature triggering of the reduction, hence, common equipment such as high-speed impeller mixers and ball mills were not chosen. A horizontal spiral ribbon mixer was

chosen, and this is suitable for processes with mixing times between 30 min and 2 h, with a maximum specific power requirement of 12 kW/m³ ³³. The purchased cost was calculated based on this power requirement.

3.4 Rotary kiln furnace

The reactants have to be under an inert atmosphere during the heating stage. It was recently shown that a tumbling motion of the powders during the reduction process helped to minimise reaction mass transfer limitations, enabling better heat dissipation and a higher yield to be achieved²². Based on these conditions, a demand of silicon of between 100 - 1500 kg/batch and ease of loading and unloading such a large quantity of particulate material, an indirect-fired rotary kiln was chosen. In this type of kiln, the reactants are sealed within a cylinder and is heated from the outside, allowing the flame to be isolated from the reactants. Given the reducing atmosphere and batch operation requirements, few other furnaces are suited for the MgTR at large scale. Another important requirement is that the reactant mixture needs to be agitated to promote mass transfer processes. Conveyor-belt type furnaces that operate under a reducing atmosphere is an alternative³⁴, however the powder is moved along a belt, rather than being mixed. At lower temperatures, a fluidised bed is another alternative however this type of equipment is more suitable for rapid reactions and it would require a large amount of reducing gas and would be uneconomical. The rotary kiln furnace can be operated in batch or continuous mode, under reducing or oxidising atmospheres, and are employed in other sectors for reduction reaction, making it a well-developed piece of equipment ³⁵. Specifications obtained from a rotary kiln furnace supplier³⁶ indicated that a throughput of 91 kg/h – 18 Mt/h could be achieved with an indirect-fired rotary kiln, and the demand of silicon calculated here falls comfortably within these limits. The sizing factor for this piece of equipment was its maximum power output, and this was used to calculate the purchased cost of the kiln³¹. For heat loss calculations, a maximum rotational speed of 17 rpm was used, as this was recently reported to give a significant increase in yield compared to a stationary reaction.

3.5 Stainless steel vessel

A glass-lined stainless-steel reactor was chosen for the dissolution step due to the requirement of aqueous HCl. The sizing factor was its volume, calculated based on the molar quantity of HCl required for a batch of a certain size, and the concentration used. The cost of the reactor based on its volume and including the impeller was estimated³².

3.6 Plate filter

The selection criteria for filters described in²⁹ was used. Based on experimental observations, settling of the solids can be seen if the mixture is left unstirred for an hour, indicating that the particles are flocculated. The solids can be effectively filtered using a cellulose paper with a nominal retention of 11 μm . While the mixture is initially an opaque brown colour, the filtrate is clear. The solids exhibit a slow settling behaviour of <0.1 cm/s, and a slow filtering behaviour in the order of cm/h. These filtration characteristics indicate that a plate filter is suitable for this process. The sizing factor used for the filter was the filter area. A filter area was calculated from the quantity of solids that needed to be filtered, along with a nominated filter cake thickness of 3 cm. The cost was found using a plate filter design chart³².

3.7 Tray dryer

Industrial drying, in principle, requires the wet powder or cake to be spread over a large surface area and hot, dry air to be passed over it. The sizing factor for a stacked, cabinet dryer was its surface area, and the cost of this equipment was calculated using the costing equation from³¹.

3.8 Indexed capital cost and annual fixed cost

The capital cost includes the combined cost of all the major equipment selected for this process. A Lang factor was applied to estimate a delivered cost³¹. The latest available Chemical Engineering Process Cost Index (CEPCI) was applied to estimate a present-day cost (indexed capital cost, ICC). Due to the requirement of handling corrosive material, a cost factor of 3.2 was applied to the ICC to calculate the inside battery limit (ISBL). From this, the outside battery limit (OSBL) was estimated, and combined with ISBL to give a total capital cost. Factors accounted for under fixed costs (FC) include operator salaries, maintenance, property taxes, rent of land, plant overheads and

environmental costs. These were estimated based on the total capital cost³¹ and are recurring every year. Dividing the total capital cost by the typical payback time of 10 years and 15% annual interest rate³¹, an adding this to the FC gives the annual FC. The specific FC in \$/kg Si was found by dividing the annual fixed cost by the annual Si production target.

3.9 Variable cost of production

The amount of energy and feedstock required to produce silicon contribute to the variable cost (VC) of the process. This cost was therefore heavily influenced by the conditions and efficiencies of the process. For the spiral powder mixer and stainless-steel vessel, typical power requirements quoted in the literature were used to estimate the total amount of energy consumed for 1 batch. For simplicity, it was assumed the plate filter separated the solids by gravity.

Energy is required in the ramping stage of the heating step to increase the temperature of the rotary kiln furnace and the reactants to the maximum reduction temperature (sensible heat). During both the ramp and dwell stages, heat is lost through conduction, convection and radiation. To calculate this, the surface area of the kiln was required, so a cylindrical geometry was assumed, with a typical length to diameter (L/D) ratio of 5. Therefore, the total energy required by the kiln included sensible heat, plus the heat lost during the ramp and dwell stages.

The final major equipment which contributed to the energy cost was the tray dryer. Energy is required to drive off moisture from the filter cake. The physical process occurring during the drying of the product were split into the following components: increase in temperature of the solvent in the filter cake to its boiling point, increase in temperature of the solid to the solvent boiling point (both sensible heat), and vaporisation of the solvent at boiling point (latent heat). The total heat supplied was calculated based on a typical energy efficiency of 80%. The methods of energy consumption of each major equipment are summarised in Table 1.

4. Results

4.1 Baseline energy costs

The baseline conditions were chosen to be 650°C maximum reduction temperature, 5°C/min ramp rate and 6-hour dwell time. These conditions are seen throughout the literature, with slight variations whereby a higher temperature of 750°C or longer dwell time of 7 hours are used. In the heating step, energy was required in the dwell and ramp stages.

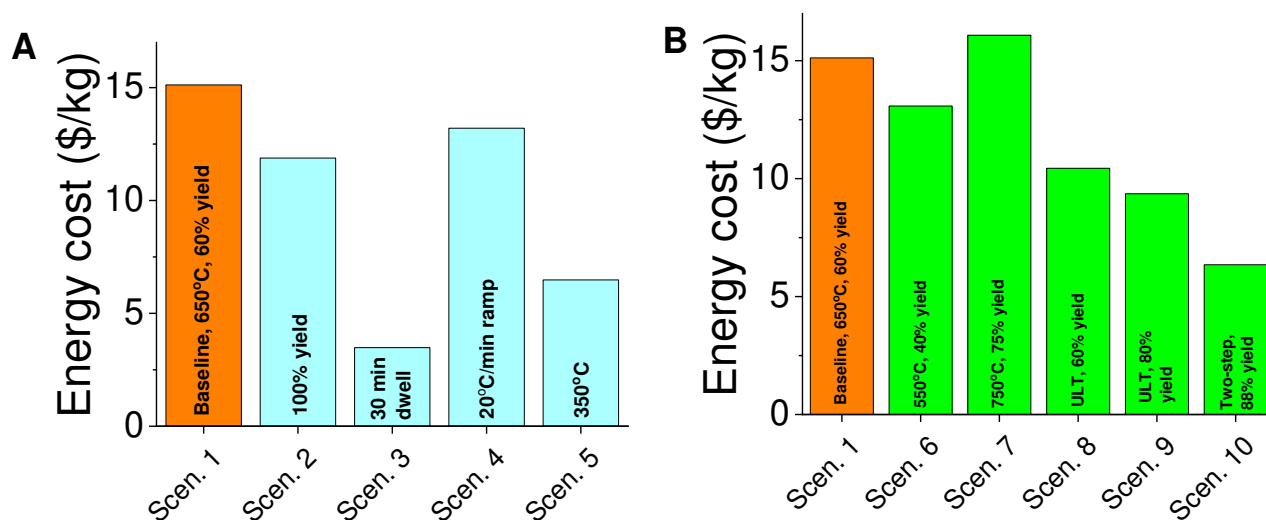


Figure 3: Total energy costs for A) hypothetical scenarios with improvements made on the baseline conditions and B) scenarios with reaction conditions and results obtained in this work and reported in the literature. Reactions carried out in the lab were at 1g scale, and these values were calculated assuming the same conditions for a 200 kg/batch scale.

Hypothetical scenarios were created by changing one condition of Scenario 1 at a time (yield, dwell time, ramp rate or reaction temperature, see Table 2), while keeping the rest constant (Fig. 3A). This helped identify the conditions which, if changed, would have the greatest impact on the specific energy cost.

The specific energy cost was calculated based on the amount of Si formed so an increase in the yield would lead to a lower energy cost. Scenario 2 is a hypothetical case to consider if the yield were to increase to 100%. In practice this would mean an improvement would need to be made to the reaction kinetics/mass transfer, and should a perfect yield be achieved, the cost would only decrease to \$11.90/kg Si. Scenario 3 is another hypothetical case with some basis from reported experiments and it was created to explore the impact of the reaction time alone on the energy cost. It had been reported in the literature that Si was formed in as little as 30 minutes at 650°C¹⁷, hence this dwell time was chosen. Note that in those studies, the yield was not accurately reported, hence we assumed an unchanged

60% yield from Scenario 1, in order to elucidate the effect of the dwell time alone on the energy cost.

Lowering the dwell time to 30 minutes (Scenario 3) resulted in a decrease in energy cost from \$15.20 to \$3.50/ kg Si. Energy is also consumed during the ramp stage, however, Scenario 4 indicates that increasing the ramp from 5°C to 20°C/min changed the cost minimally from \$15.20 down to \$13.20 /kg Si. While the traditional MgTR had not been reported to be feasible at 350°C, it had recently been shown to proceed at a similar temperature of 380°C ²¹. The scenario with the second lowest energy cost of \$6.50 /kg Si was Scenario 5 with reaction temperature reduced to 350°C. These results were expected as lowering the furnace temperature, and the time spent at high temperatures would give the greatest decrease in energy consumption. This analysis helped identify the dwell time and reaction temperature as the key contributors to the energy demands of the process.

Table 2: A summary of various MgTR process scenarios used in this study. Any parameters changed from the baseline Scenario 1 are shown in bold.

Scenario	Reaction temperature °C	Dwell time h	Yield %	Ramp rate °C/min	Energy cost \$/kg Si
Scenario 1	650	6	60	5	15.20
Scenario 2	650	6	100	5	11.90
Scenario 3	650	0.5	60	5	3.50
Scenario 4	650	6	60	20	13.20
Scenario 5	350	6	60	5	6.50
Scenario 6	550	6	40	5	13.08
Scenario 7	750	6	75	5	16.10
Scenario 8	380	6	60	5	10.44
Scenario 9	380	6	80	5	9.40
Scenario 10	650, 300*	0.5, 6	88	5	6.40

**Unlike all other scenarios, this required a two-step process at two different temperatures.*

It is well known that the yield of the traditional, one-step reaction increases with the maximum furnace temperature¹⁹. Scenario 6 and 7 showed the energy cost of the reduction based on data reported in²¹, see Figure 4b. While an increase in furnace temperature from 650 to 750°C had been shown to give a higher yield, it was not enough to outweigh the cost of the temperature increase, hence the cost also increased (\$16.10). Simply increasing the yield by increasing the temperature would have an effect on the pore properties and performance of the material, which is not reflected in a techno-economic analysis. It is also important to mention that while a decrease in temperature from 650 to 550°C did lower energy costs, the yield also suffered, which would also affect the performance of the material. Given that the use of HF is to be avoided, the unreacted SiO₂ would remain in the final

product. While a yield of 40% would still result in a high anode capacity, the high amount of SiO₂ would hinder access to Si by the Li, so a capacity of less than 40% would be observed. Next, the energy costs for two recently discovered low-temperature experimentally validated scenarios were compared (Fig. 3B). From the results of the hypothetical scenarios, it was to be expected that scenarios with lower reduction temperatures and dwell times would have the greatest reduction in cost compared to Scenario 1. Scenario 10 was the two-step method which was described in our previous work²⁰, and showed the highest cost decrease, from Scenario 1 down to \$6.40 /kg Si. Scenario 8 represented the ultra-low temperature (ULT) process described in our previous work²¹. Scenario 9 represented a hypothetical method with improved yield from Scenario 8 and shows the second highest cost decrease down to \$9.40 /kg Si.

It is therefore clear that to have the greatest impact on process economics of the MgTR, the maximum temperature, or time spent at maximum temperature should be lowered. This should be done while maintaining or improving the yield and structural properties of the product so that a high performance can still be achieved. Scenario 9 and Scenario 10 have the lowest energy costs and the highest yields of the various scenarios presented. Therefore, the rest of the techno-economic analysis will focus only on these two scenarios. The cost of Scenario 1 method will also be included for comparison.

4.2 Energy costs improvements

In order to identify potential improvements for the Scenarios 9 and 10, we investigated the impact of temperature and time. For the ULT process (Scen. 9), most of the energy was consumed in the dwell step. The dwell step accounted for 91% of the energy consumption (Fig. S1A). Halving the dwell time from 6 hours to 3 hours at 380°C lowered the energy cost from \$9.40 /kg Si to \$ 5.50 /kg Si (Fig. 4A), whereas remaining at 6 hours but drastically dropping the temperature from 380 to 300°C only lowers the energy cost to \$7.00 /kg Si. This shows that decreasing the dwell time had a greater impact on the energy cost than decreasing the maximum temperature.

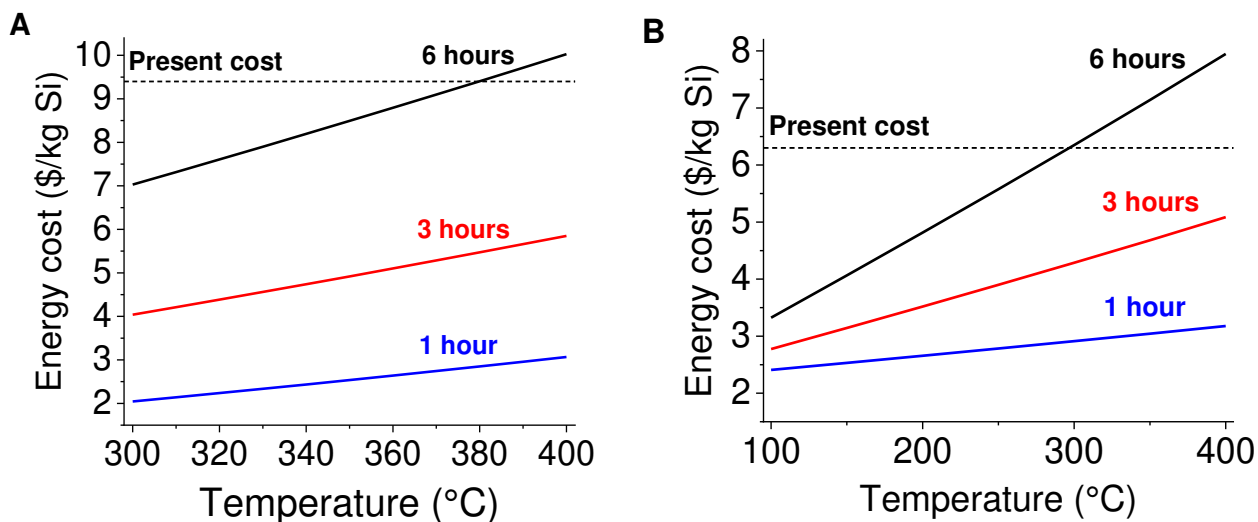


Figure 4: The energy cost for A) ULT process for different dwell times and B) the two-step process with different 2nd step dwell time and temperatures are shown.

From Fig. S1B, the second dwell time consumed the most energy in Scenario 10. Fig. 4B shows the effect of changing dwell time and temperature of the second step on the total energy cost of the process. If higher temperatures cannot be avoided, then a lower dwell time should be used. For example, at 300°C, the cost can be brought down from \$6.30 at 6 hours to \$4.30 and \$2.90 /kg Si at 3 hours and 1 hour respectively. It may be that a higher temperature would be required to improve mass transfer and cut reaction time. In this case, increasing the reaction to 400°C while decreasing the dwell time to 3 hours or below would still lower energy costs.

These results aid direct future experimental work in optimising time and temperature to give the greatest economic benefit. In practice, improving the reaction in favour of economics requires experimental investigations to understand the reaction pathways and include other key product attributes such as porosity, purity, crystallinity and performance.

4.3 Feedstock costs

To complete the calculation of the variable cost, the feedstock cost was estimated. Mg is the most expensive feedstock, with a unit cost of \$4100 /ton³⁷. It is not as abundant as SiO₂ and is required in its elemental form, which does not occur naturally. The change in total feedstock cost based on the unit cost of Mg is shown in Fig. S2. For a method with a higher yield, the increase in Mg cost has less

of an effect on the total feedstock cost, than a method with a lower yield. In the MgTR, a minimum stoichiometric amount of 2:1 moles Mg:SiO₂ will always be required, and usually an excess of 2.2:1 - 2.5:1 is used. Decreasing the amount of Mg below the stoichiometric requirement would cause the yield of Si to suffer, however using a lower excess would lower feedstock costs.

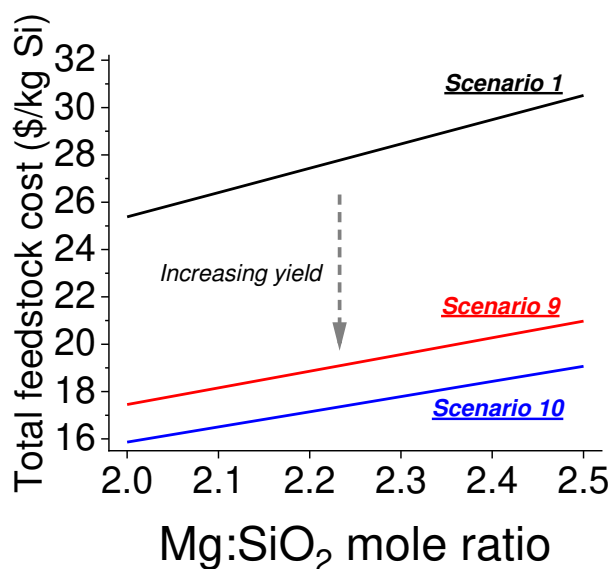


Figure 5: The total feedstock cost Scenario 1, Scenario 9 and Scenario 10 at different molar ratios of Mg:SiO₂ above the stoichiometric requirement are compared.

For any given mole ratio, the differences in cost between the scenarios seen in Fig. 5 were due to the yield of Si achieved. Using a high mole ratio of 2.5:1 in Scenario 9 or 10 still resulted in a much lower total feedstock cost than Scenario 1 due to the high yield that can be achieved. This highlights the importance of yield on the total feedstock cost. While it is clear that lowering the Mg:SiO₂ ratio is important for lowering costs, there are practical issues that arise when using lower mole ratios, such as lower Mg diffusivity and rate of reaction, or the formation of by-products. In order to keep feedstock costs low, it is primarily important that a high yield is achieved, and secondarily that a low Mg:SiO₂ ratio is used.

4.4 Lowering feedstock costs

Given the already high yield of Scenario 9, increasing the yield further has less of an impact on the cost of the Mg, and changing the Mg:SiO₂ has a comparable effect (Fig. 6A). If a lower Mg:SiO₂ ratio could be used to achieve a yield of 80%, while still avoiding the formation of by-products, the cost

could be lowered from \$21.00 /kg Si to \$17.50 /kg Si. On the other hand, in order to achieve a similar cost savings while using a high mole ratio of 2.5:1, the yield would have to be increased to above 95%.

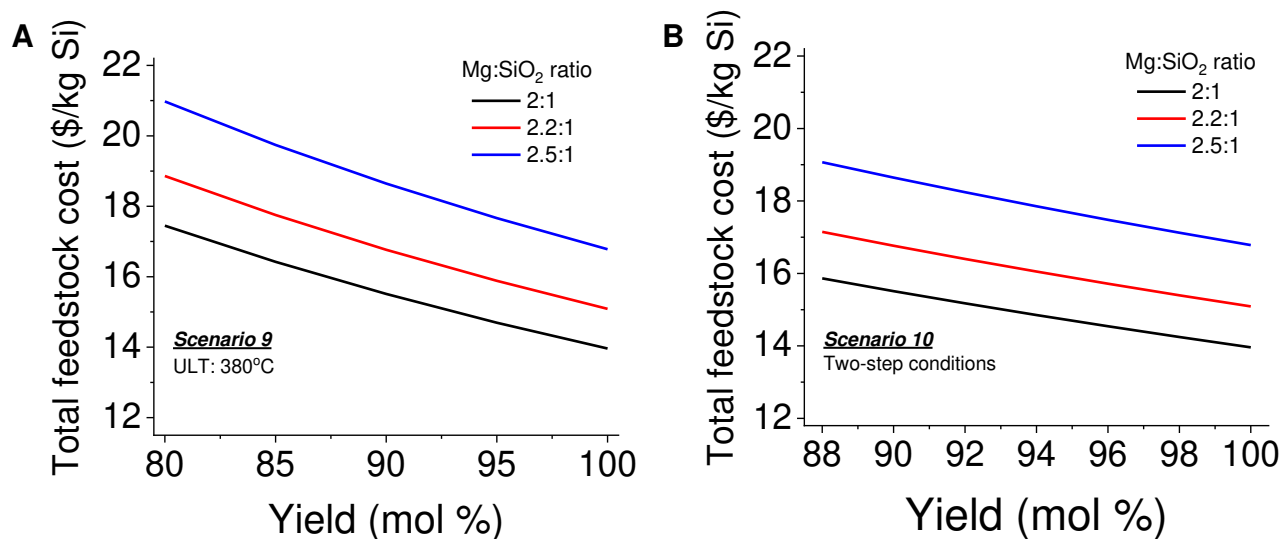


Figure 6: The feedstock cost at different hypothetical yields and Mg:SiO₂ mole ratios for the ULT process are given in A, and for the two-step process are given in B.

Practically it may be possible to achieve a high yield using a low mole ratio through better mixing (prior to heating or in-situ) in order to promote mass transfer and avoid locally high concentrations of SiO₂ or Mg. Similarly to Scenario 9, the already high yield achieved in Scenario 10 meant that little savings to feedstock cost could be made as the yield approaches 100% (Fig. 6B). Decreasing the mole ratio of Mg:SiO₂ below 2.2:1 also gave little savings, and the only clear benefit of using a lower mole ratio would mean better protection against Mg cost fluctuations. The data presented in Fig. 7 show that savings from the feedstock costs were low (~17%), compared to the possible savings from the energy cost seen in Fig. 5. This conclusion would need to be reconsidered should the cost of Mg feedstock in practice increase far beyond the \$4/kg used for these calculations.

4.5 Fixed cost

The equipment costs were firstly estimated based on key design requirements and costing factors (Table 1). Factors were applied to the capital cost include installation and delivery costs. The Process

Cost Index (CEPCI) for 2020 (596.2) was applied giving the ICC. Fig. 7A shows the proportion that each equipment contributes to the ICC. The capital cost of each equipment was dependent on the total mass, and therefore volume of the reactants required. These conditions were themselves dependent on the yield of the reaction, and a lower yield would mean more feedstock required to produce a given mass of p-Si compared to the same reaction with a higher yield. Tap densities of the feedstock are also important as they affect the required equipment volume and hence the capital cost. The capital cost of the kiln was calculated based on a power output factor. The maximum power output for each scenario was calculated using the rate of heat loss at the maximum temperature, taking into account the amount of surface area of the kiln. Given that Scenario 9 required a maximum temperature of only 380°C compared to Scenario 1 and 10 (both at 650°C), the cost of the kiln for Scenario 9 was the lowest of the three. The lined vessel, dryer and filter had cost factors which were based on the mass and volume of the solid products being handled. Scenario 1, with the lowest yield, would require the most SiO₂ and Mg to produce the same mass of Si as Scenario 9 and 10. In order to remove the unreacted Mg, a greater amount of HCl would be required from Scenario 1, hence, a larger lined vessel volume.

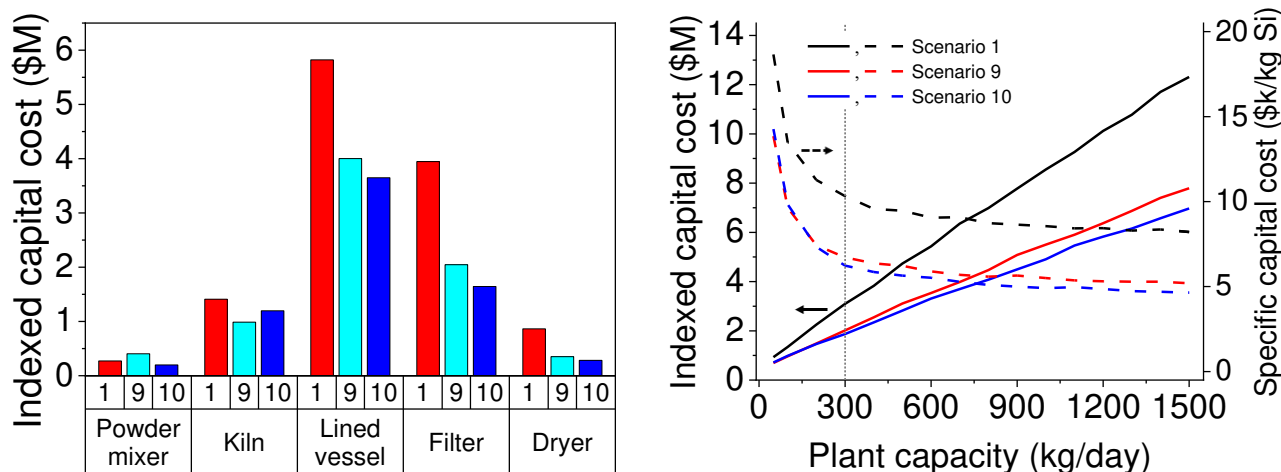


Figure 7: A) Indexed capital cost of individual equipment for Scenarios 1, 9 and 10 at the 1500 kg scale. B) Solid lines represent indexed capital costs, while broken lines represent specific capital costs at different plant capacities. The vertical line marks 300 kg/d beyond which the ICC does not change significantly.

The tray dryer and filter were sized according to surface area required. Similar to the lined vessel, the amount of powder was used in the calculations. A lower yield resulted in a greater amount of SiO₂

remaining in the product, which meant greater surface areas were needed to spread the powder during the filtering and drying stages. For these reasons, the cost of the filter and dryer were highest in Scenario 1, and lowest in Scenario 10. Due to the relatively lower yield achieved in Scenario 1, the ICC is higher overall than Scenarios 9 and 10 (Fig. 7B). All 3 Scenarios show similar decrease in the specific capital cost with scale indicating economies of scale, however this effect diminishes beyond ~300 kg/d production rates.

4.6 Total cost of production (TCOP)

From the ICC, the annual fixed cost associated with the running of the plant was estimated according to the flow diagram presented in Fig. 2. A payback time of 10 years at 15% interest rate was assumed, which corresponds to an annual capital charge ratio (ACCR) of 0.199. The annual fixed cost for each scenario was normalised to the amount of Si produced in the year, giving a fixed cost in \$/kg Si. This was added to the variable costs (feedstock and energy costs) to give the TCOP, at different batch sizes between 100 and 1500 kg (Fig. 8).

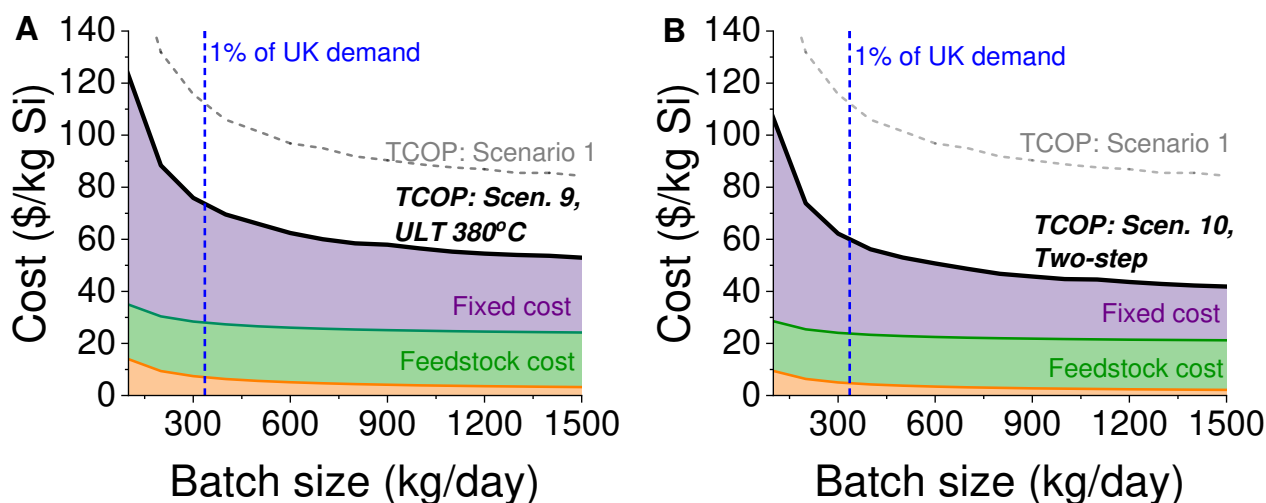


Figure 8: Feedstock cost, FC and TCOP for A) Scenario 9 and B) Scenario 10, compared to the TCOP of Scenario 1 at different scales. Orange area represents energy costs.

The TCOPs of Scenarios 9 and 10, for a scale equivalent to 1% of the UK demand determined in this work, were below \$70-85 /kg. This was far below Scenario 1, which was \$126 /kg. At this scale, the fixed costs made up the majority of the cost at all scales, but this proportion decreased at larger

scales, indicating the potential for a larger profit margin at larger scales. It is worth noting that, from the information available in the public domain, the price of C-coated Si anodes was determined to be \$200 /kg³⁸. At a scale of 1500 kg/day, the TCOP for Scenarios 1, 9 and 10 were \$85 /kg, \$53 /kg and \$42 /kg, respectively, which are far below the \$200/kg market price, highlighting the cost competitiveness of the MgTR even under the baseline conditions. While it is important to maintain materials performance during scale-up, it is well known that economy of scale typically reduces the costs even further.

While the energy cost made up the lowest proportion in the TCOP, the parameters set for the reaction will have an impact at the design stage of the process, determine the size and cost of the equipment required, and impact the fixed cost of the process. Table S1 summarises how changing reaction parameters, in particular, the yield and maximum temperature, will affect the cost of equipment.

4.7 Equipment cost improvements

Fig. 8 presented in the previous section showed that the most expensive piece of equipment was the lined vessel. The proportion of the total cost of this equipment was greater than 50% for both Scenario 9 and Scenario 10 (Fig. S3). The cost of this equipment was based on its volume. For a given amount of Mg used in the process, a corresponding amount of HCl is always required in the etching process, at a molar ratio of 1:2 Mg:HCl. The volume of HCl required is therefore dependent on the concentration of the acid used. The total volume, and cost of the dissolution vessel could be minimised by increasing the concentration of acid used. The greatest improvement can be seen by increasing the molar concentration of acid from 1M, that is currently reported in the literature, to 5M (Fig. 9). This corresponded to a decrease in TCOP of approximately 20% for Scenario 9 and Scenario 10 for a given production rate. However, combining the economy of scales and increasing HCl concentration shows that at least 50% reduction in TCOP can be achieved (see Table 3). It is expected that the rate of dissolution of Mg species would increase with concentration of HCl, which would decrease the overall duration of the MgTR, thus further reducing the production costs.

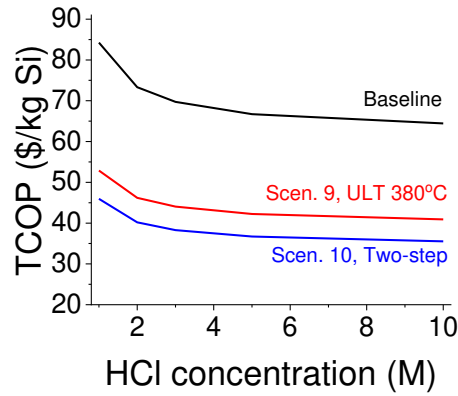


Figure 9: Change in TCOP with increasing HCl concentration used in the etching step at 1500 kg scale.

Table 3: Summary of the TCOP in \$/kg Si at 200 kg and 1500 kg scale using 1M or 5M HCl concentrations.

Scenario	200 kg scale		1500 kg scale	
	1M HCl	5M HCl	1M HCl	5M HCl
1	132	114	84	67
9	88	78	53	42
10	84	75	46	37

4.8 Capacity cost

Here, the cost of p-Si will be considered in the context of anodes for lithium-ion cells and will be compared to graphite on a cost per capacity basis rather than simply cost of production per mass. This approach has the advantage of providing strong comparison with existing technologies on the basis of performance, hence helping to identify potential market opportunities. To compare the cost of p-Si to that of graphite, the specific costs/selling price of these materials were converted to a per-capacity basis. The selling price of natural spherical graphite was reported to be \$3/kg³⁹. Using a capacity of 350 mAh/g this was equivalent to a capacity cost of 0.85 cent/Ah.

While porous Si is more resistant to degradation upon lithiation when compared to non-porous Si particles, partial lithiation is known to limit the degradation of Si and capacity fade⁴⁰. Hence, we considered the capacity cost of Si obtained from Scenarios 9 and 10 for a range of partial lithiation states (Fig. 10). The yields of each scenario were taken into account when calculating capacity cost. For example, p-Si made in Scenario 9 (80% yield) and lithiated to 50% would be able to achieve 1431 mAh/g. This calculation was performed for a range between 20-70% lithiation for Scenarios 9 and 10. It was assumed that the cell would be able to maintain its capacity at its given percent lithiation in

every cycle beyond cycle 100. Under this assumption, a material that did not have any capacity fade from degradation in the first 100 cycles would have a % lithiation of 100%. As this is unrealistic, a conservative limit of 70% lithiation is used. The cost at a 1500 kg scale is competitive with graphite even when lithiation is limited to 30% (around 4 cents/Ah). This cost further decreases to 2 cents/Ah at 70% lithiation. Going down from 30 to 20%, the cost almost doubles to nearly 8 cents/Ah. Below 20% lithiation the cost would increase by a greater amount, and this would be equivalent to a capacity <math><572 \text{ mAh/g}</math>.

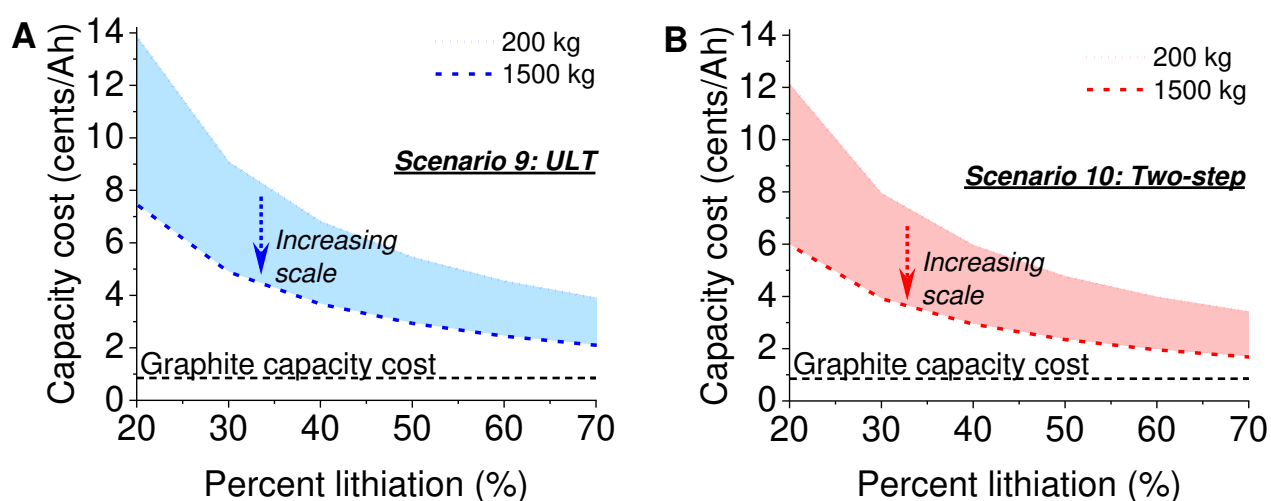


Figure 10: Capacity cost of p-Si made by the A) ULT and B) Two-step processes at scales between 200 and 1500 kg, assuming the p-Si is lithiated to percentages between 20 and 70%.

4.9 Sensitivity analysis

The effect of changing each parameter on the cost of the process were individually calculated in the previous sections. To compare the effects of the different variables, a sensitivity analysis was carried out for Scenarios 9 and 10 between -30 and +30% of their base conditions (Fig. 11A and B). Increasing the yield had the greatest immediate effect on the TCOP, however the yield can only reach a maximum of 100%, which sets the lower limit of \$46 and \$42/kg for Scenario 9 and 10 respectively. Changing the HCl concentration has the second greatest effect on the cost of the process. While the upper limit for the increase in concentration presented in Fig. 11 is +30%, it was shown in Fig. 9 that the cost can be lowered further by increasing the concentration to 5M (by 400%) and beyond.

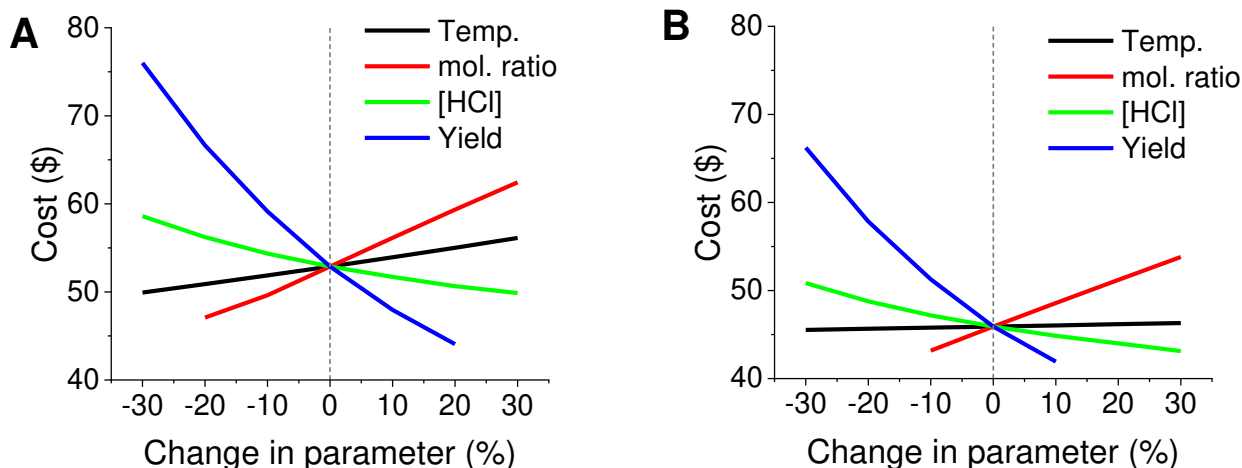


Figure 11: A sensitivity analysis was performed for A) Scenario 9 and B) Scenario 10. The temperature, mole ratio, HCl concentration and yields were varied independently between -30 and +30% of their respective conditions. The mole ratios were limited at the lower percentage due to minimum stoichiometric requirements, while the yield was limited at the upper range as it cannot exceed 100%.

Given that the energy cost was the smallest portion of the TCOP, and that the temperatures of Scenario 9 and 10 were already low, lowering the temperature by 30% had the smallest effect on the TCOP, relative to the other 3 variables. Fundamentally, the yield is dependent on the mole ratio and temperature, as well as other reaction variables. The sensitivity analysis shows that drop in yield is the most detrimental to the TCOP, so if it can be avoided by increasing the mole ratio or temperature, it is worthwhile doing so from an economic perspective.

5. Conclusion

We present the first techno-economic study of p-Si production using magnesiothermic reduction process in order to assess its competitiveness as well as inform future research and development required in the field. The total cost of producing p-Si via the MgTR at batch sizes between 200-1500 kg was calculated and presented. We found that energy costs accounted for the smallest proportion of the total cost of production, and the two-step process had the lowest energy cost of \$6.40/kg Si, followed by the ultra-low temperature one-step method (\$9.40/kg Si). The biggest savings in energy cost achieved can be between 33-55% by decreasing second step dwell time from 6h to between 3-1 h. Magnesium was identified as the most expensive feedstock, and the yield of reaction made the biggest difference to the overall feedstock cost. Fixed cost accounted for the biggest proportion of the

total production cost and it was dependent on the cost of the equipment. The most expensive piece of equipment was the lined vessel required for washing of unreacted Mg, the MgO product and any by-products, and it accounted for over 50% of the indexed capital cost. We identified that increasing the acid concentration used in this washing step would require a smaller lined vessel, with the potential to a decrease in total cost of production by 20%. Incorporating such improvements, we calculated the TCOP at 1500 kg/day scale to be \$42 and \$37/kg for the ultra-low temperature and two-step reduction methods respectively. When considering together the production costs and performance of p-Si produced, the energy storage 'capacity cost' was found to be between 2 and 4 cents/Ah for both the ultra-low temperature and the two-step methods. Our study provides a reasonable estimate which indicates that the MgTR process is cost competitive and scalable method for producing Si, and with recent advancements such as the ultra-low temperature and two-step methods, the total cost of producing decreases drastically. Suggestions on ways to lower the cost of production further have been provided by understanding the impact of various conditions and parameters. Future work should focus on identifying ways to practically implement improvements while keeping in mind their implications on process economics.

6. Acknowledgements

We thank the following funders for supporting this research: EPSRC (EP/P006892/1 and EP/R025983/1), the CDT for Energy Storage and its Applications (EP/L016818/1), the Faraday Institution (Seed Project), UKRI-Mitacs Globalink Doctoral Exchange (NE/V02129X/1) and Invest Nova Scotia for Postdoctoral funding. MY would also like to thank Matthew Garayt and Reid Dressler for helpful discussions. SM would like to thank NSERC Alexander Graham Bell Canada Graduate Scholarship-Doctoral (CGS D) and Walter C. Sumner Memorial Fellowship for graduate funding. MD would like to thank Killam Trusts for financial support.

References

- 1 Faraday Report Annual Gigafactory Study, *UK electric vehicle and battery production potential to 2040*, 2020.
- 2 Nissan Leaf Specifications, https://www.nissan.co.uk/vehicles/new-vehicles/leaf.html#C400_cmp_story_839a-modal, (accessed 22 May 2022).
- 3 US Department of Energy, Samm Gillard, 2021.
- 4 European Technology and Innovation Platform, *Batteries Europe Strategic Research Agenda*, 2020.
- 5 D. W. Olson, R. L. Virta, M. Mahdavi, E. S. Sangine and S. M. Fortier, *Geological Society of America*, 2016, **520**, 66–67.
- 6 M. N. Obrovac, L. Christensen, D. B. Le and J. R. Dahn, *J Electrochem Soc*, 2007, **154**, A849–A855.
- 7 M. N. Obrovac and L. Christensen, *Electrochemical and Solid-State Letters*, 2004, **7**, A93.
- 8 J. Moon, H. C. Lee, H. Jung, S. Wakita, S. Cho, J. Yoon, J. Lee, A. Ueda, B. Choi, S. Lee, K. Ito, Y. Kubo, A. C. Lim, J. G. Seo, J. Yoo, S. Lee, Y. Ham, W. Baek, Y. G. Ryu and I. T. Han, *Nature Communications 2021 12:1*, 2021, **12**, 1–10.
- 9 C. Wang, H. Wu, Z. Chen, M. T. Mcdowell, Y. Cui and Z. Bao, *Nat Chem*, 2013, **5**, 1042–1048.
- 10 M. N. Obrovac and L. J. Krause, *J Electrochem Soc*, 2007, **154**, A103.
- 11 H. Wu, G. Zheng, N. Liu, T. J. Carney, Y. Yang and Y. Cui, *Nano Lett*, 2012, **12**, 904–909.
- 12 N. Liu, L. Hu, M. T. McDowell, A. Jackson and Y. Cui, *ACS Nano*, 2011, **5**, 6487–6493.
- 13 H. Wu, G. Chan, J. W. Choi, I. Ryu, Y. Yao, M. T. Mcdowell, S. W. Lee, A. Jackson, Y. Yang, L. Hu and Y. Cui, *Nature Nanotechnology 2012 7:5*, 2012, **7**, 310–315.
- 14 D. H. Filsinger and D. B. Bourrie, *Journal of the American Ceramic Society*, 1990, **73**, 1726–1732.
- 15 D. Losic and A. Santos, *Electrochemically engineered nanoporous materials*, 2015.
- 16 Z. Bao, M. R. Weatherspoon, S. Shian, Y. Cai, P. D. Graham, S. M. Allan, G. Ahmad, M. B. Dickerson, B. C. Church, Z. Kang, H. W. Abernathy, C. J. Summers, M. Liu and K. H. Sandhage, *Nature*, 2007, **446**, 172–175.
- 17 D. Cho, M. Kim, J. Hwang, J. H. Park, Y. L. Joo and Y. Jeong, *Nanoscale Res Lett*, 2015, **10**, 1–8.
- 18 J. Entwistle, A. Rennie and S. Patwardhan, *J Mater Chem A Mater*, 2018, **6**, 18344–18356.
- 19 J. E. Entwistle, G. Beaucage and S. V. Patwardhan, *J Mater Chem A Mater*, 2020, **8**, 4938–4949.
- 20 S. A. Martell, Y. Lai, E. Traver, J. MacInnis, D. D. Richards, S. MacQuarrie and M. Dasog, *ACS Appl Nano Mater*, 2019, **2**, 5713–5719.
- 21 M. Yan and S. V. Patwardhan, *RSC Adv*, 2021, **11**, 35182–35186.
- 22 N. Yoon, C. Young, D. H. Kang, H. Park and J. K. Lee, *Electrochim Acta*, 2021, **391**, 138967.

- 23 Z. Favors, W. Wang, H. H. Bay, Z. Mutlu, K. Ahmed, C. Liu, M. Ozkan and C. S. Ozkan, *Sci Rep*, 2014, **4**, 5623.
- 24 C. Li, C. Liu, W. Wang, Z. Mutlu, J. Bell, K. Ahmed, R. Ye, M. Ozkan and C. S. Ozkan, *Sci Rep*, 2017, **7**, 1–11.
- 25 J. Ryu, D. Hong, S. Choi and S. Park, *ACS Nano*, 2016, **10**, 2843–2851.
- 26 Advanced Propulsion Centre, *Q4 2022 Automotive industry demand forecast*, 2022.
- 27 Northern Graphite Corporation, Graphite Growth Markets, <https://www.northerngraphite.com/about-graphite/graphite-growth-markets/lithium-ion-batteries/>, (accessed 21 April 2023).
- 28 K. Liebscher, The Li-ion battery in the electric car Nissan Leaf contains nearly 40 kg of graphite, <https://www.evwind.es/2012/09/05/the-li-ion-battery-in-the-electric-car-nissan-leaf-contains-nearly-40-kg-of-graphite/22953>, (accessed 21 April 2023).
- 29 D. W. Green and M. Z. Southard, *Perry's Chemical Engineers' Handbook*, McGraw-Hill Education, New York, Ninth Edit., 2019.
- 30 J. R. Couper, W. R. Penney, J. R. Fair and S. M. Walas, *Chemical Process Equipment: Selection and Design*, Elsevier, Oxford, Third Edit., 2012.
- 31 R. K. Sinnott and G. Towler, *Chemical Engineering Design*, Elsevier Ltd, Oxford, Fifth Edit., 2009.
- 32 M. Peters and K. D. Timmerhaus, *Plant Design and Economics for Chemical Engineers*, McGraw-Hill, Inc, Singapore, Fourth Edi., 1991.
- 33 E. Paul, V. A. Atiemo-Obeng and S. M. Kresta, *Handbook of Industrial Mixing: Science and Practice*, John Wiley & Sons Ltd, New Jersey, 2004.
- 34 P. Mullinger and B. Jenkins, *Industrial and Process Furnaces: Principles, Design and Operation: Second Edition*, 2013.
- 35 A. A. Boateng, *Rotary Kilns: Transport Phenomena and Transport Processes: Second Edition*, 2015, 1–368.
- 36 Feeco International, Indirect fired rotary kilns, <https://feeco.com/rotary-kilns/>, (accessed 21 April 2023).
- 37 Lee Bray, *Mineral Commodity Summaries - Magnesium Metal*, 2022.
- 38 Xiamen TOB New Energy Technology Co., Ltd., https://www.tobmachine.com/lithium-ion-battery-carbon-coated-silicon-as-si-anode-material_p917.html, (accessed 9 June 2022).
- 39 Benchmark Mineral Intelligence, Graphite demand from lithium-ion batteries to more than treble in 4 years, <https://www.benchmarkminerals.com/blog-archive/graphite-demand-from-lithium-ion-batteries-to-more-than-treble-in-4-years/>, (accessed 21 April 2023).
- 40 D. Jantke, R. Bernhard, E. Hanelt, T. Buhrmester, J. Pfeiffer and S. Haufe, *J Electrochem Soc*, 2019, **166**, A3881–A3885.

Supplementary Information

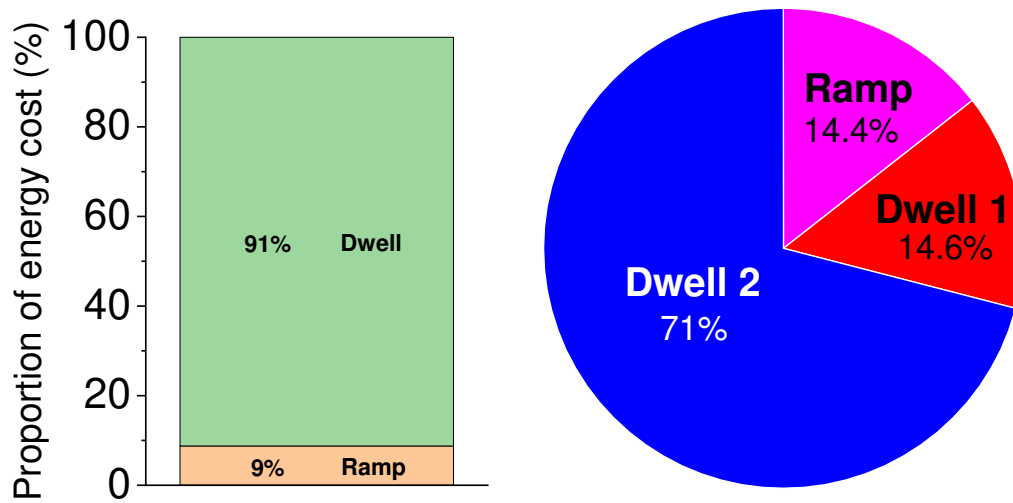


Figure S1: Proportion that each step that requires energy input contributes to the total energy cost.

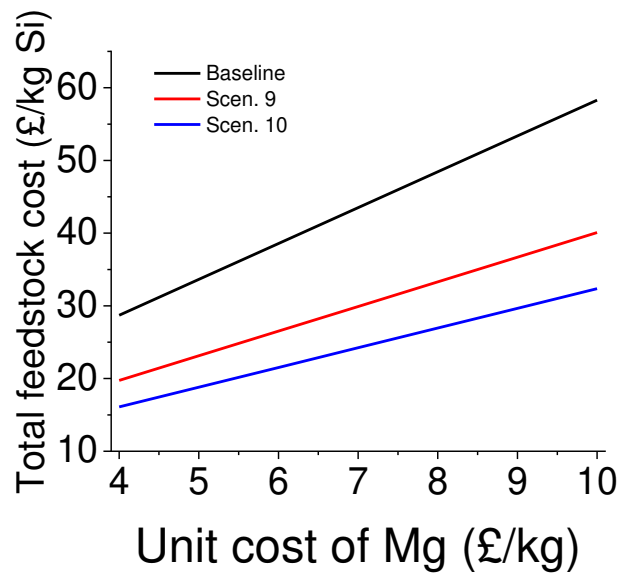


Figure S2: Effect of unit cost of Mg on the total feedstock cost.

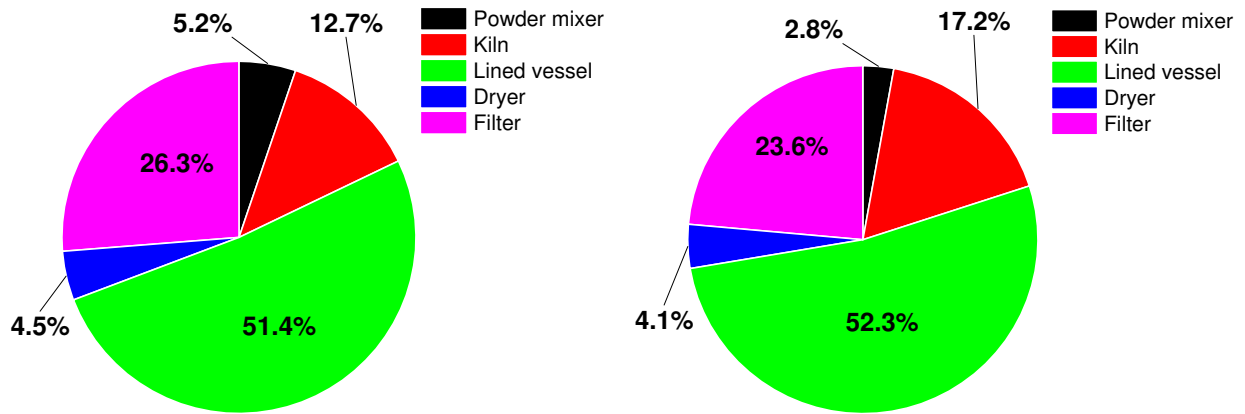


Figure S3: Pie chart showing the cost contribution of each equipment to the total capital cost for A) Scenario 9 and B) Scenario 10.

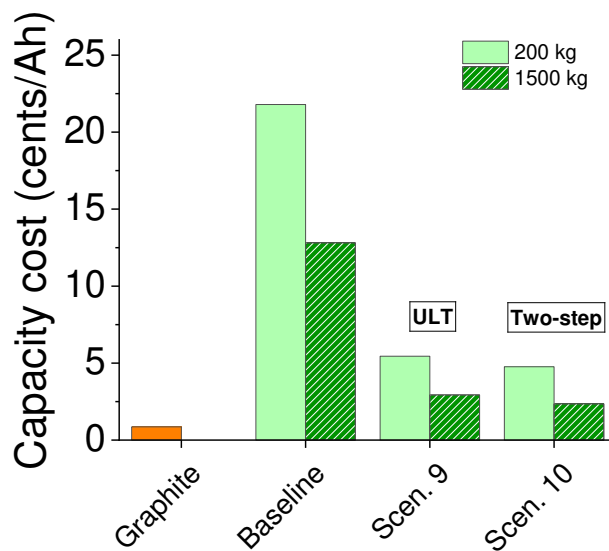


Figure S4: Capacity cost of graphite vs silicon made by the baseline, ULT and two-step magnesiothermic reduction methods.

Table S1: A summary of the parameters which determine the energy cost which also affect equipment cost.

Parameter changed	Effect on process	Equipment affected	Costing factors
Lowering temperature	Lower heat loss	Rotary kiln	Lower max. power output
Increasing yield	Less feedstock required, lower heat loss	All	Lower: max. power output, max. volume, surface area